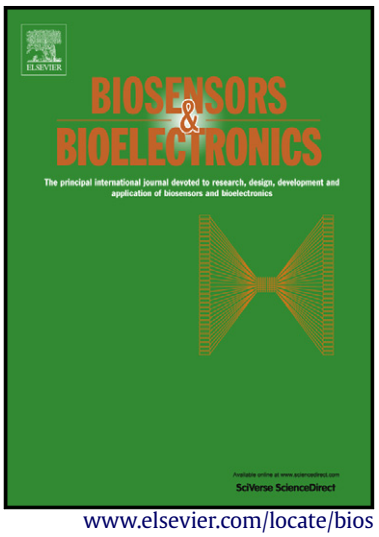

www.elsevier.com/locate/bios

Molecularly imprinted electrochemical biosensor based on Fe@Au nanoparticles involved in 2-aminoethanethiol functionalized multi-walled carbon nanotubes for sensitive determination of cefexime in Human plasma

Mehmet Lütfi Yola, Tanju Eren, Necip Atar

PII: S0956-5663(14)00312-1
DOI: http://dx.doi.org/10.1016/j.bios.2014.04.045
Reference: BIOS6749

To appear in: *Biosensors and Bioelectronics*

Received date: 25 February 2014
Revised date: 10 April 2014
Accepted date: 22 April 2014

Cite this article as: Mehmet Lütfi Yola, Tanju Eren, Necip Atar, Molecularly imprinted electrochemical biosensor based on Fe@Au nanoparticles involved in 2-aminoethanethiol functionalized multi-walled carbon nanotubes for sensitive determination of cefexime in Human plasma, *Biosensors and Bioelectronics*, http://dx.doi.org/10.1016/j.bios.2014.04.045

Molecularly imprinted electrochemical biosensor based on Fe@Au nanoparticles involved in 2-aminoethanethiol functionalized multi-walled carbon nanotubes for sensitive determination of cefexime in human plasma

Mehmet Lütfi Yola[a*], Tanju Eren[b], Necip Atar[b]

[a]*Sinop University, Faculty of Engineering, Department of Metallurgical and Materials Engineering, Sinop, Turkey*
[b]*Dumlupınar University, Faculty of Arts and Sciences, Department of Chemistry, Kutahya, Turkey*

***** To whom correspondence should be addressed:

Dr. Mehmet Lütfi YOLA

Sinop University

Faculty of Engineering

Department of Metallurgical and Materials Engineering

Tel.: +903682715761; Fax: +903682715763

E-mail: mehmetyola@gmail.com

ABSTRACT

The molecular imprinting technique depends on the molecular recognition. It is polymerization method around the target molecule. Hence, this technique creates specific cavities in the cross-linked polymeric matrices. In present study, a sensitive imprinted electrochemical biosensor based on Fe@Au nanoparticles (Fe@AuNPs) involved in 2-aminoethanethiol (2-AET) functionalized multi-walled carbon nanotubes (f-MWCNs) modified glassy carbon (GC) electrode was developed for determination of cefexime (CEF). The results of x-ray photoelectron spectroscopy (XPS) and reflection–absorption infrared spectroscopy (RAIRS) confirmed the formation of the developed surfaces. CEF imprinted film was constructed by cyclic voltammetry (CV) for 9 cycles in the presence of 80 mM pyrrole in phosphate buffer solution (pH 6.0) containing 20 mM CEF. The developed

electrochemical biosensor was validated according to the International Conference on Harmonisation (ICH) guideline and found to be linear, sensitive, selective, precise and accurate. The linearity range and the detection limit were obtained as 1.0×10^{-10} - 1.0×10^{-8} M and 2.2×10^{-11} M, respectively. The developed CEF imprinted sensor was successfully applied to real samples such as human plasma. In addition, the stability and reproducibility of the prepared molecular imprinted electrode were investigated. The excellent long-term stability and reproducibility of the prepared CEF imprinted electrodes make them attractive in electrochemical sensors.

Keywords:

Molecularly imprinting; Cefexime; Fe@Au nanoparticles; Multi-walled carbon nanotubes; Validation; Human plasma

1. Introduction

Cephalosporins with β-lactam ring interfere with the synthesis of the bacterial cell wall. They are used for the treatment of infections caused by Gram (+) and Gram (−) bacteria. They are one of the most effective antimicrobial agents. Hence, they are the most frequently prescribed as class of antibiotics (Shah 2002; Williams et al. 2001). CEF (Scheme 1) is a semi-synthetic and generally classified as a third-generation cephalosporin antibiotic. It is used for the treatment of infections including gonorrhea, lower respiratory-tract infections such as bronchitis and urinary-tract infections (Sweetman 2002). The various analytical methods such as liquid chromatographic–tandem mass spectrometric (LC–MS–MS) (Meng et al. 2005), high-performance liquid chromatography (HPLC) (Nemutlu et al. 2009), differential pulse cathodic adsorptive stripping voltammetry (DPCAdSV) (Jain et al. 2010), square-wave voltammetry (SWV) (Afkhami et al. 2013), CV (Ensafi and Allafchian 2013), high-performance capillary electrophoresis (Honda et al. 1992), spectrophotometric (Shah and Pundarikakshudu 2006) and spectrofluorimetric (Shah et al. 2011) have been developed for

determination of CEF. But these methods have some disadvantages such as large material consumption and expensive equipment.

The carbon nanotubes have good conductivity, chemical stability and mechanical strength (Ajayan 1999). They have significant applications such as electron field emission sources (Heer et al. 1995), nanoelectronic devices (Tans et al. 1998), batteries (Che et al. 1998) and chemical sensors (Gupta et al. 2013a; Gupta et al. 2013b). In addition, they can enhance electron-transfer on electrochemical reactions (Yola and Atar 2014). The core/shell nanoparticles are important functional materials (Ghosh Chaudhuri and Paria 2011). They are used in various applications such as biomedical (Balakrishnan et al. 2009), pharmaceutical applications (Caruso 2001) and catalysis (Daniel and Astruc 2003).

Although the various methods are used to increase the sensitivity, the most effective method is molecular imprinting technique. The method relies on the molecular recognition. It is a kind of polymerization which is formed around the target molecule. Hence this technique forms specific cavities in the cross-linked polymeric matrices (Bonini et al. 2007). Molecular imprinted polymers (MIPs) have various applications such as artificial enzymes (Bonini et al. 2007), solid-phase extraction (Esen et al. 2009), bioseparation (Asliyuce et al. 2013; Bereli et al. 2008; Saylan et al. 2012; Uzun et al. 2009a), affinity detoxification (Andac et al. 2004; Erturk et al. 2011) and sensor devices (Diltemiz et al. 2009; Gupta et al. 2014b; Uzun et al. 2009b; Yola et al. 2014a; Yola et al. 2014c).

A novel GC surface based on Fe@AuNPs involved in 2-AET functionalized f-MWCNs was developed in present study. The surface was firstly developed via electrochemical modification. After that, Fe@AuNPs and 2-AET functionalized f-MWCNs were self-assembled onto the developed surfaces. The surfaces were characterized by using scanning electron microscope (SEM), CV, electrochemical impedance spectroscopy (EIS), XPS and RAIRS. The molecular imprinted polymer on the novel surface was formed and

applied as a molecular recognition element for highly sensitive and selective determination of CEF. By this way, we aimed to prepare homogeneous polymeric film surface which is an important property to achieve repeatable, accurate and trustable sensor responses. The proposed method is precise, accurate, sensitive, rapid, cheap and easy and might be preferred to published chromatographic and spectrophotometric methods. In addition, the method provides a novel efficient protocol for the ultrasensitive detection of CEF in human plasma.

2. Experimental

2.1. Chemicals and materials

CEF, cefepime (CEP), cefotaxime (COT) and cefoperazone (COP) were purchased from Fargem Company (Düzce, Turkey) and used as received. The stock solution of CEF (1.0 mM) was prepared by dissolving it in 5 mL of ultra pure quality water and then diluting it with ultra pure quality water to 25 mL. The working solutions were prepared by diluting the stock solution with 0.10 M phosphate buffer (pH 6.0). The MWCNTs of 30-40 nm in diameter and 1.0-5.0 μm in length; purity: ≥ 95% were purchased from Sigma–Aldrich. p-nitroaniline (Merck), tetrabutylammoniumtetrafluoroborate (TBATFB) (Sigma–Aldrich, USA), pyrrole (Sigma–Aldrich), hydrogen tetra-chloroaurate hydrate ($HAuCl_4$) (Sigma–Aldrich, USA), iron(III) nitrate [$Fe(NO_3)_3$] (Sigma–Aldrich, USA), 2-AET (Sigma–Aldrich, USA), ascorbic acid (Sigma–Aldrich, USA), N-(3-dimethylaminopropyl)-N′-ethylcarbodiimidehydrochloride (EDC) (Sigma–Aldrich, USA), potassium ferricyanide ($K_3[Fe(CN)_6]$) (Sigma–Aldrich, USA), potassium ferrocyanide ($K_4[Fe(CN)_6]$) (Merck), potassium chloride (KCl) (Merck, Germany), HPLC grade acetonitrile (MeCN) (Sigma–Aldrich, USA), isopropyl alcohol (IPA) (Sigma–Aldrich, USA), sulphuric acid (H_2SO_4) (Sigma–Aldrich, USA), nitric acid (HNO_3) (Sigma–Aldrich, USA), activated carbon (Sigma–Aldrich, USA), sodium chloride (NaCl) (Merck, Germany) and other chemicals were reagent grade quality. The preparation of the aqueous solutions was performed by using ultra pure

quality of water with a resistance of 18.3 MΩ cm (Human Power 1^{+} Scholar purification system).

2.2. Instrumentation

All electrochemical measurements were performed by using IviumStat (U.S) equipped with C3 cell stand.

Electrochemical impedance spectroscopic experiments were performed with IVIUMSTAT & IVIUMSTAT.XR: Electrochemical Interface & Impedance Analyser. The electrodes were characterized in 1.0 mM $Fe(CN)_6^{3-/4-}$ redox couple. EIS data were measured at 100 kHz to 0.1 Hz at wave amplitude of 10 mV and at an electrode potential of 0.165 V.

The infrared spectra were recorded with Bruker Tensor 27 FT-IR DTGS detector by using a Ge total reflection accessory.

XPS analysis was performed on a PHI 5000 Versa Probe (Φ ULVAC-PHI, Inc., Japan/USA) model X-ray photoelectron spectrometer instrument with monochromatized Al Kα radiation (1486.6 eV) as an X-ray anode operated at 50 W. The sample was prepared on a clean glass slide by placing one drop of the nanostructure and then allowing it to air dry.

TEM measurements were performed on a JEOL 2100 HRTEM instrument (JEOL Ltd., Tokyo, Japan) to examine the morphology of Fe@AuNPs.

SEM is ZEISS EVO 50 analytic microscope (GERMANY).

All the pH measurements were performed with Mettler Toledo MA 235.

2.3. Cleaning procedure for GC electrodes

GC electrodes were cleaned by polishing them with fine wet emery paper (grain size 4000). The electrodes were polished successively in 0.1 μm and 0.05 μm alumina slurries (Baikowski Int. Corp., U.S) on microcloth pads (Buehler, Lake Bluff, IL, U.S). The electrodes were sonicated in ultra pure water and in 50:50 (v/v) IPA + MeCN solution purified over activated carbon two times, respectively. After removal of trace alumina from the surface by

rinsing with water, they were rinsed with MeCN to remove any physisorbed or unreacted materials. The reference electrode was either a $Ag/AgCl/KCl_{(sat)}$ used in aqueous media or a Ag/Ag^{+} (0.01 M) used in MeCN. The counter electrode was a Pt wire.

2.4. Preparation of NP/GC and AP/GC electrodes

After GC electrodes were cleaned, the electrodes were dried using argon gas. The surface derivatization was performed in 1.0 mM of p-nitrophenyl diazonium tetrafluoroborate salt in MeCN with 0.1 M TBATFB using CV at a scan rate of 100 mV s^{-1} between +0.60 V and -0.60 V. p-nitrophenyl diazonium salt was synthesized from p-nitroaniline (Haque et al. 2012). After the formation of p-nitrophenyl (NP) modified GC (NP/GC) electrode, it was scanned negatively to reduce the nitro groups to amine in 0.01 M HCl for the preparation of p-aminophenyl (AP) modified GC (AP/GC) electrode at a scan rate of 100 mV s^{-1} between -0.20 V and -1.40 V.

2.5. Functionalization of MWCNTs

100 mg of MWCNTs was treated with 10 mL of concentrated HNO_3+H_2SO_4 (3:1) (v/v) for 24 h. After sonication, the mixture was filtered and washed several times with ultra pure water until a pH level of 6.5-7.0 was reached. The f-MWCNTs were dried at 120^{o}C for 6 h. This treatment was performed to open the ends of carbon nanotubes and add carboxylic groups on the surface of carbon nanotubes (Janegitz et al. 2011).

2.6. Preparation of f-MWCNs/AP/GC electrode

After preparation of the AP/GC electrode and f-MWCNs, AP/GC electrode was sonicated in water and then in MeCN to send away the adventitious adsorption of species for 10 min. To ensure the surface activation of carboxylate groups of f-MWCNs, the AP/GC electrode was immersed in f-MWCNs solution (2.0 mg mL^{-1}) containing 0.2 M EDC for 12 h (***f-MWCNs/AP/GC***).

2.7. Preparation of Fe@AuNPs

To prepare the Fe@AuNPs, $Fe(NO_3)_3$ (4 mL, 0.01 M) was reduced by 20 mL of 0.1 M ascorbic acid for about 20 min at room temperature under a nitrogen flow. The pH of the solution was adjusted around 4.0 and the $HAuCl_4$ (4 mL, 0.01 M) was added at room temperature for 1 h. A dark solid confirmed that the iron core was coated with gold shell. Then, the product was separated by a magnet and washed with water. The Fe@AuNPs were dried in a vacuum oven at 25^{o}C (Gupta et al. 2014a).

2.8. Preparation of Fe@AuNPs/2-AET-f-MWCNs/AP/GC

To ensure the surface activation of carboxylate groups of f-MWCNs/AP/GC electrode, f-MWCNs/AP/GC electrode was interacted with 0.2 M EDC solution for 12 h. The activated f-MWCNs/AP/GC electrode was well mixed with 1.0 mM 2-AET for 3 h (***2-AET-f-MWCNs/AP/GC***). In a typical experiment of self-assembly, 2-AET-f-MWCNs/AP/GC electrode was dipped into aqueous dispersion of Fe@AuNPs (4.0 mg mL^{-1}) and washed with water for 15 min (***Fe@AuNPs/2-AET-f-MWCNs/AP/GC)***. The modified electrodes were stored in ultra pure quality of water without fluctuations of temperature and pressure.

2.9. Preparation of CEF imprinted sensor

The schematic diagram of the preparation of CEF imprinted biosensor is shown in Scheme 1. The CEF imprinted film on Fe@AuNPs/2-AET-f-MWCNs/AP/GC (***MIP/Fe@AuNPs/2-AET-f-MWCNs/AP/GC***) electrode was prepared by using CV for 9 cycles in the presence of 80 mM pyrrole in phosphate buffer solution (pH 6.0) containing 20 mM CEF at a scan rate of 100 mV s^{-1} between 0.0 V and +1.00 V. CEF imprinted electrochemical biosensor was soaked in pH 6.0 of phosphate supporting electrolyte to remove non-polymeric pyrrole from the electrode surface.

A control experiment, non-imprinted polymer modified electrode (NIP), was prepared under the same experimental conditions without adding CEF to check the reliability of the measurements.

2.10. CEF removal from electrode surface

There are the electrostatic interactions and hydrogen bonding between pyrrole monomer and polar groups of CEF molecules. In order to break the interactions, we used 1.0 M NaCl solution in water as a desorption agent. Firstly, the removal study of CEF was performed via batch system. CEF imprinted electrochemical surface was dipped into 25 mL of desorption agent. The electrode was swinged in bath (200 rpm) at room temperature. After CEF removal, the electrode was washed with ultra pure quality water and dried under vacuum (200 mmHg, 25^{o}C).

2.11. Sample preparation

1.2 mL methanol were added to an aliquot of 0.4 mL human plasma sample in a 2.0 mL plastic centrifuge tube. After that, the centrifugation at 20000 rpm for 15 min was performed. The upper clear layer solution was diluted with phosphate buffer (pH 6.0) for analysis.

Here Scheme 1

3. Results and discussion

3.1. The formation of the developed surfaces by CV

GC electrodes were electrochemically modified with 1.0 mM p-nitrophenyl diazonium tetrafluoroborate salt in MeCN. Fig. 1A shows a cyclic voltammogram for the modification of p-nitrophenyl to the GC electrode. The first sweep showed the characteristic reduction peak at about -0.20 V. The subsequent scans showed a passivated electrode (Liu et al. 2005). The multicycled modification voltammogram is very characteristic for the reduction of diazonium salt. The irreversible reduction wave of diazonium salt is indicative of the formation of 4-nitrophenyl radical followed by covalent binding to the carbon surface (Liu and McCreery 1995; Matrab et al. 2007). Fig. 1B shows the surface voltammogram indicating the reduction

of surface nitro groups to the amino groups with 6 electron transfer (Üstündağ and Solak 2009; Yu et al. 2007). After the preparation of Fe@AuNPs/2-AET-f-MWCNs/AP/GC surface, the pyrrole polymer (PPy) film was formed onto the Fe@AuNPs/2-AET-f-MWCNs/AP/GC to obtain MIP/Fe@AuNPs/2-AET-f-MWCNs/AP/GC surface. The MIP/Fe@AuNPs/2-AET-f-MWCNs/AP/GC electrode was obtained in potential range between 0.0 V and +1.0 V during 9 cycles (scan rate 100 mV s^{-1}) (Fig. 1C) in the phosphate electrolyte including (1:4) mole ratio of CEF molecule to pyrrole monomer. As shown in Fig. 1C, the peak current decreased with the increasing of CV cycles, indicating that the imprinted film was successfully deposited on the electrode surface. During the electropolymerization process, the CEF molecules diffuse towards the surface of Fe@AuNPs/2-AET-f-MWCNs/AP/GC electrode and trapped in the PPy matrix owing to ability of these molecules to interact with pyrrole. Hence, the transfer of electron was obstructed between the electrode surface and analyte molecules. Finally, the imprinted electrode was rinsed with 1.0 M NaCl solution in water as a desorption agent to remove the template CEF for 30 min.

Here Fig. 1A, Fig. 1B and Fig.1C

3.2. Characterization

The morphologies of the surfaces in present study were characterized by SEM. A smooth surface was observed in the SEM image of bare GC surface (Fig. 2A). The some slices were covered on the GC surface (Fig. 2B), which indicated the successful modification of GC electrode with p-aminophenyl group. The SEM image of f-MWCNs/AP/GC indicated that the distribution of carbon nanotubes on the AP/GC surface was very smooth and homogeneous with typical nanotube morphology (Fig. 2C). After modification of Fe@AuNPs on the 2-AET-f-MWCNs/AP/GC electrode, a dense layer of spherical Fe@AuNPs was

covered on the 2-AET-f-MWCNs/AP/GC surface, indicating that the successful binding of Fe@AuNPs (Fig. 2D). After electropolymerization process of pyrrole was completed, a layer of electrodeposition was covered onto the Fe@AuNPs/2-AET-f-MWCNs/AP/GC surface, indicating that the imprinted electrochemical biosensor was successfully prepared (Fig. 2E).

Here Fig. 2

Fig. S1A shows the TEM image of Fe@AuNPs. TEM image confirms spherical shapes. In the Fe@AuNPs morphology, the darker nucleus assigns to the iron nanoparticle and the lighter shell assigns to the gold nanoparticle. EDX analysis confirmed the formation of Fe@AuNPs/2-AET-f-MWCNs/AP/GC surface. The C, Au, Fe and S peaks have been observed in EDX analysis (Fig. S1B).

The RAIRS measurements (Fig. 3A) and XPS characterization (Fig. S2) confirm the formation of the Fe@AuNPs/2-AET-f-MWCNs/AP/GC surface. The peaks at 286.9, 284.6 and 283.4 eV are corresponded to –CONH, C–O or C–N and C–H, respectively (Yola et al. 2014b). The N_{1s} narrow region spectrum of the surface is curve-fitted and the peak at 398.6 eV is attributed to the amide's N–H groups which consist of a reaction of the carboxyl group of the f-MWCNs with the amino group of the 2-AET. The peak at 400.4 eV is assigned to the N-H group of unreacted 2-AET molecules. The appearance of sulphur peaks at 162.8 and 162.1 eV confirm the binding of sulphur to the gold atom. The Au $4f^{7/2}$ peak signal at 83.1 eV confirms the presence of bonded Au. It is also possible that the signal at 88.6 eV is due to unreacted gold nanoparticles (AuNPs) (Yola and Atar 2014). The peaks of Fe $2p^{1/2}$ and Fe $2p^{3/2}$ appear at 713.1 and 710.8 eV, respectively. These peaks indicate the presence of iron nanoparticles (Gupta et al. 2014c).

The RAIRS spectrum reveals the characteristic stretching vibrations of NH_2 (N–H, around 3360 cm^{-1}), aromatic C-H (3040 cm^{-1}) and aromatic C=C (1570 cm^{-1}) on the AP/GC surface (curve a of Fig. 3A). The characteristic stretching vibrations of C=O (COOH) (1520 cm^{-1}) and C-N (1280 cm^{-1}) confirm the presence of f-MWCNs attached to AP/GC surface (curve b). The peaks at 2980 cm^{-1}, 1190 cm^{-1} and 1310 cm^{-1} are corresponded to aliphatic C-H, C-S and C-N on Fe@AuNPs/2-AET-f-MWCNs/AP/GC surface, respectively. In addition, the existence of the band at 3520 cm^{-1} for the N–H stretching vibration verifies the covalent functionalization of the carboxyl group of the f-MWCNs with 2-AET (Yola and Atar 2014).

Cyclic voltammograms of MIP and NIP films in 1.0 mM $[Fe(CN)_6]^{3-/4-}$ solution containing 0.1 M KCl were recorded at the scan rate of 100 mV s^{-1} (Fig. 3B and 3C). It was obvious that the cyclic voltammogram of bare GC electrode (curve a of Fig. 3B) showed a well-defined reversible peaks of 1.0 mM $[Fe(CN)_6]^{3-/4-}$ with 200 mV of peak potential difference (ΔEp). In spite of the observation of a reversible redox wave on the bare GC electrode, the peaks are completely blocked at AP/GC electrode (curve b of Fig. 3B). After covalently rebinding of f-MWCNs to AP/GC electrode, a increase in the peak current with ΔEp = 160 mV was observed (curve c of Fig. 3B). The modification of AuNPs on the 2-AET-f-MWCNs/AP/GC electrode decreased ΔEp with a small increase in the peak current (curve d of Fig. 3B), indicating that AuNPs increased the effective surface area of electrode. The oxidation peak current of 1.0 mM $[Fe(CN)_6]^{3-/4-}$ greatly increased on Fe@AuNPs/2-AET-f-MWCNs/AP/GC electrode (curve e of Fig. 3B), indicating that Fe@AuNPs/2-AET-f-MWCNs nanocomposite effectively increased the electrode active area and catalytic activity (Gupta et al. 2014a). For MIP/Fe@AuNPs/2-AET-f-MWCNs/AP/GC electrode, the blockage of oxidation and reduction of 1.0 mM $[Fe(CN)_6]^{3-/4-}$ (from curve e to curve f) was due to the formation of PPy film, which blocked electron transfer. After the removing of CEF, a visible oxidation-reduction peak was observed (curve g of Fig. 3B). This situation is owing to the

removed templates making electronic transfer possible. The peak current from curve g to curve h decreased because the holes of PPy structure were filled. Hence, the electron transfer of $[Fe(CN)_6]^{3-/4-}$ redox couple was again blocked.

As shown in Fig. 3C, well-defined reversible peaks of 1.0 mM $[Fe(CN)_6]^{3-/4-}$ were observed on bare GC electrode (curve a of Fig. 3C). The curve b of Fig. 3C showed reversible peaks of 1.0 mM $[Fe(CN)_6]^{3-/4-}$ on Fe@AuNPs/2-AET-f-MWCNs/AP/GC electrode. Because the PPy film covered the surface of the GC electrode in the absence of CEF, the reversible peaks of 1.0 mM $[Fe(CN)_6]^{3-/4-}$ on the NIP/Fe@AuNPs/2-AET-f-MWCNs/AP/GC electrode decreased dramatically from curve b to curve c. Hence, NIP/Fe@AuNPs/2-AET-f-MWCNs/AP/GC electrode was unselective and unrecognizable.

EIS is an effective method for probing the features of modified surfaces. Fig. 3D shows the EIS of Fe@AuNPs/2-AET-f-MWCNs/AP/GC electrode (curve a of Fig. 3D), MIP/Fe@AuNPs/2-AET-f-MWCNs/AP/GC electrode without elution (curve b of Fig. 3D) and MIP/Fe@AuNPs/2-AET-f-MWCNs/AP/GC electrode after the removing of CEF (curve c of Fig. 3D) in 1.0 mM $[Fe(CN)_6]^{3-/4-}$ (1:1) solution in 0.1 M KCl. The values of charge transfer resistance (R_{ct}) were calculated for Fe@AuNPs/2-AET-f-MWCNs/AP/GC electrode, MIP/Fe@AuNPs/2-AET-f-MWCNs/AP/GC electrode after elution and MIP/Fe@AuNPs/2-AET-f-MWCNs/AP/GC electrode as 35.0 ohm, 45.0 ohm and 60.0 ohm, respectively. After an electrochemical imprinted film was electrodeposited on the Fe@AuNPs/2-AET-f-MWCNs/AP/GC electrode, the semicircle diameter increased. This case was assigned to the covering of the PPy. When the CEF was removed from the surface, the R_{ct} was smaller than the R_{ct} of MIP/Fe@AuNPs/2-AET-f-MWCNs/AP/GC electrode without elution. It was owing to the elution of the template CEF molecule resulting in increment of the electron transfer rate.

CEF exhibits a well-defined oxidation peak, which is owing to the oxidation of 2-aminothiazole group (Golcu et al. 2005). As shown in Fig. 3E, the oxidation peaks of CEF at 0.95 V were observed at the MIP/Fe@AuNPs/2-AET-f-MWCNs/AP/GC, Fe@AuNPs/2-AET-f-MWCNs/AP/GC, 2-AET-f-MWCNs/AP/GC, NIP/Fe@AuNPs/2-AET-f-MWCNs/AP/GC and bare GC electrodes. The oxidation peak is not observed at the NIP/Fe@AuNPs/2-AET-f-MWCNs/AP/GC electrode (curve e) since the non-imprinted polymer has no cavities for binding CEF. In addition, the higher oxidation current of MIP/Fe@AuNPs/2-AET-f-MWCNs/AP/GC electrode (curve a of Fig. 3E) indicated that the binding capacity of MIP/Fe@AuNPs/2-AET-f-MWCNs/AP/GC electrode was better. Finally, the above analysis confirmed that the MIP/Fe@AuNPs/2-AET-f-MWCNs/AP/GC electrode had special recognition capacity towards CEF molecule and the recognition capacity was due to the imprinted effect.

Here Fig. 3A, Fig. 3B, Fig. 3C, Fig.3D and Fig. 3E

3.3. Optimization of analytical conditions

3.3.1. The effect of the concentration of Fe@AuNPs

The effect of the concentration of Fe@AuNPs was tested on the response of the MIP/Fe@AuNPs/2-AET-f-MWCNs/AP/GC electrode. The peak current of CEF increased with increasing of the concentration of Fe@AuNPs up to 4.0 mg mL^{-1}. However, after the concentration exceeded 4.0 mg mL^{-1}, the peak current of CEF was almost constant. Hence, 4.0 mg mL^{-1} of Fe@AuNPs was selected as optimum amount (Fig. 4A).

3.3.2. The *effect of pH*

The pH of the medium has important influence on the polymeric film. Fig. 4B showed the dependence of the peak current on the pH in the range of 4.0-8.0. The best response was

observed at pH 6.0 according to the lowest non-impriting response. According to the results, CEF molecules which are specific adsorbed to the imprinted binding sites show different electrochemical oxidation behaviors in different pHs.

3.3.3. The effect of the mole ratio of CEF molecule to pyrrole monomer

The effect of the mole ratio of CEF molecule to pyrrole monomer was investigated in the range from 1:2 to 1:7 (Fig. 4C). The results showed that the peak current of CEF increased when the ratio was reduced and it achieved a maximum at 1:4. This was related to the change of the number of available binding site. When the amount of pyrrole monomer was little, the number of available binding site was few. However, a high concentration of the monomer might cause a nonselective electrochemical response. The mole ratio of 1:4 was optimal and chosen.

3.3.4. The effect of elution time

Fig. 4D showed the effect of elution time. The peak current of CEF increased with the elution time up to the 30 min and remained constant subsequently. Hence, the elution time of 30 min was selected in the subsequent experiments.

Here Fig. 4

3.4. Validation of the proposed molecular imprinting method

3.4.1. Linearity range

The square wave voltammograms recorded with increasing amount of CEF (Fig. 5A) showed that the peak currents increased linearly with increasing concentration. Each point of the calibration graph was corresponded to the mean value from six independent measurements. The regression equation of CEF (Fig. 5B) is $y = 0.962x + 0.266$. Table S1 gives the data of the calibration curve.

Here Fig. 5A, Fig. 5B and Fig. 5C

Limit of quantification was estimated by the equation:

$$LOQ = 10\ S / m,$$

Limit of detection was estimated by the equation**:**

$$LOD = 3.3\ S / m,$$

Where *S* is the standard deviation of the intercept and *m* is the slope of the regression line (Gustavo González and Ángeles Herrador 2007). LOQ and LOD were found to be 1.0×10^{-10} M and 2.2×10^{-11} M, respectively.

3.4.2. Precision

Three different concentrations of CEF (0.1, 1.0, 5.0 nM) in the linear range were analyzed in six independent series on the same day (intra-day precision) and six consecutive days (inter-day precision) (Table S2). The relative standard deviation (RSD) values varied from 0.61 to 0.91 for intra-day and from 0.47 to 0.87 for inter-day precision. The low RSD values of intra-day and inter-day indicated that the developed method had a high precision (Green 1996).

3.4.3. Accuracy

Accuracy was evaluated as a percentage of relative error between the measured mean concentrations and added concentrations for CEF (Bias %). Both the results obtained for intra-day and inter-day accuracy were ≤ 1.00 % (Table S2) (Green 1996).

3.4.4. Recovery

The recovery experiments in human plasma samples were performed with different CEF concentrations. The results are presented in Table S3. The closeness of the results to

100.00 % showed that recovery of the CEF imprinted electrochemical biosensor was very good.

A rapid, simple and sensitive LC–MS–MS method was employed as a comparison to evaluate the validity of the imprinted electrochemical method (Meng et al. 2005). Table S4 gives the results obtained by the two methods for the determination of CEF in human plasma samples. These results were compared by Wilcoxon test and there was no significant difference between the obtained results of SWV and LC–MS–MS ($T_{calculated} > T_{tabulated}$, $p > 0.05$).

3.5. Selectivity, Stability and Reproducibility of the imprinted sensor

In order to investigate the selectivity of the CEF imprinted biosensor in the presence of CEP, COP and COT as competitors, the samples were applied to the CEF imprinted electrochemical biosensor. CEF imprinted biosensor was 7.1, 8.3 and 14.3 times more selective for CEF than CEP, COP and COT, respectively (Fig. 5C). The results showed that because of selective cavities in the polymer structure, the imprinted electrode possessed good selectivity. CEF imprinted biosensor shows low non-specific responses for CEP, COP and COT. These responses resulted from the structural and physico-chemical similarities between CEF and the other β-lactam antibiotics (CEP, COP and COT).

The reproducibility was estimated with six MIP/Fe@AuNPs/2-AET-f-MWCNs/AP/GC electrodes that were fabricated independently by the same procedure. The RSD is 0.39% in the presence of 1.0×10^{-8} M CEF. The low value of RSD demonstrates the reliability of the fabrication procedure. Additionally, the stability of one MIP/Fe@AuNPs/2-AET-f-MWCNs/AP/GC electrode was also investigated. After 60 days, the current response is approximately 97.08% of the original value. The excellent long-term stability and reproducibility of the prepared MIP electrodes make them attractive in the fabrication of electrochemical sensors.

3.6. Comparison of the performance of the proposed MIP sensor with other analytical systems

The performance of the fabricated electrochemical biosensor has also been compared with other analytical systems and the results are shown in Table S5. Compared with the results, the proposed biosensor showed a much lower limit of detection with high selectivity. In addition, there is the first report about determination of CEF in human plasma via molecular imprinting technology. Hence a fast, sensitive and simple imprinted electrochemical biosensor can offer new developments for detecting new β-lactam antibiotics from biological samples in the future.

4. Conclusion

A novel imprinted electrochemical biosensor based on Fe@AuNPs and f-MWCNs was developed for direct determination of CEF in human plasma. The developed electrochemical imprinted biosensor showed high sensitivity and selectivity towards CEF with a detection limit of 2.2×10^{-11} M. In particular, the developed imprinted electrochemical sensor offers the advantages of simplicity and efficiency in target detection from biological samples, which is essential for the determination of CEF. In addition, this original surface and detection method allow new β-lactam antibiotics recovery.

References

Afkhami, A., Soltani-Felehgari, F., Madrakian, T., 2013. Electrochim. Acta 103, 125-133.

Ajayan, P.M., 1999. Chem. Rev. 99(7), 1787-1800.

Andac, M., Say, R., Denizli, A., 2004. J. Chromatogr. B 811(2), 119-126.

Asliyuce, S., Uzun, L., Say, R., Denizli, A., 2013. React. Funct. Polym. 73(6), 813-820.

Balakrishnan, S., Bonder, M.J., Hadjipanayis, G.C., 2009. J. Magn. Magn. Mater. 321(2), 117-122.

Bereli, N., Andac, M., Baydemir, G., Say, R., Galaev, I.Y., Denizli, A., 2008. J. Chromatogr. A 1190(1-2), 18-26.

Bonini, F., Piletsky, S., Turner, A.P.F., Speghini, A., Bossi, A., 2007. Biosens. Bioelectron. 22(9-10), 2322-2328.

Caruso, F., 2001. Adv. Mater. 13(1), 11-22.

Che, G.L., Lakschmi, B.B., Fisher, E.R., Martin, C.R., 1998. Nature 393, 346-349.

Daniel, M.-C., Astruc, D., 2003. Chem. Rev. 104(1), 293-346.

Diltemiz, S.E., Hur, D., Ersoz, A., Denizli, A., Say, R., 2009. Biosens. Bioelectron. 25(3), 599-603.

Ensafi, A.A., Allafchian, A.R., 2013. Colloids Surf. B 102, 687-693.

Erturk, G., Uzun, L., Tumer, M.A., Say, R., Denizli, A., 2011. Biosens. Bioelectron. 28(1), 97-104.

Esen, C., Andac, M., Bereli, N., Say, R., Henden, E., Denizli, A., 2009. Mater. Sci. Eng. C Mater. Biol. Appl. 29(8), 2464-2470.

Ghosh Chaudhuri, R., Paria, S., 2011. Chem. Rev. 112(4), 2373-2433.

Golcu, A., Dogan, B., Ozkan, S.A., 2005. Talanta 67(4), 703-712.

Green, J.M., 1996. Anal. Chem. 68(9), 305A-309A.

Gupta, V.K., Atar, N., Yola, M.L., Eryılmaz, M., Torul, H., Tamer, U., Boyacı, İ.H., Üstündağ, Z., 2013a. J. Colloid Interface Sci. 406, 231-237.

Gupta, V.K., Atar, N., Yola, M.L., Üstündağ, Z., Uzun, L., 2014a. Water Res. 48, 210-217.

Gupta, V.K., Yola, M.L., Atar, N., 2014b. Sens. Actuators B 194, 79-85.

Gupta, V.K., Yola, M.L., Eren, T., Kartal, F., Çağlayan, M.O., Atar, N., 2014c. J. Mol. Liq. 190, 133-138.

Gupta, V.K., Yola, M.L., Qureshi, M.S., Solak, A.O., Atar, N., Üstündağ, Z., 2013b. Sens. Actuators B 188, 1201-1211.

Gustavo González, A., Ángeles Herrador, M., 2007. Trends Anal. Chem. 26(3), 227-238.

Haque, A.-M.J., Park, H., Sung, D., Jon, S., Choi, S.-Y., Kim, K., 2012. Anal. Chem. 84(4), 1871-1878.

Heer, W.A.D., Chatelain, A., Ugarte, D., 1995. Science 270, 1179-1180.

Honda, S., Taga, A., Kakehi, K., Koda, S., Okamoto, Y., 1992. J. Chromatogr. A 590(2), 364-368.

Jain, R., Gupta, V.K., Jadon, N., Radhapyari, K., 2010. Anal. Biochem. 407(1), 79-88.

Janegitz, B.C., Pauliukaite, R., Ghica, M.E., Brett, C.M.A., Fatibello-Filho, O., 2011. Sens. Actuators B 158(1), 411-417.

Liu, G., Liu, J., Böcking, T., Eggers, P.K., Gooding, J.J., 2005. Chem. Phys. 319(1–3), 136-146.

Liu, Y.-C., McCreery, R.L., 1995. J. Am. Chem. Soc. 117(45), 11254-11259.

Matrab, T., Save, M., Charleux, B., Pinson, J., Cabet-deliry, E., Adenier, A., Chehimi, M.M., Delamar, M., 2007. Surf. Sci. 601(11), 2357-2366.

Meng, F., Chen, X., Zeng, Y., Zhong, D., 2005. J. Chromatogr. B 819(2), 277-282.

Nemutlu, E., Kır, S., Katlan, D., Beksaç, M.S., 2009. Talanta 80(1), 117-126.

Saylan, Y., Sari, M.M., Ozkara, S., Uzun, L., Denizli, A., 2012. Mater. Sci. Eng. C Mater. Biol. Appl. 32(4), 937-944.

Shah, J., Jan, M.R., Shah, S., Inayatullah, 2011. J. Fluoresc. 21(2), 579-585.

Shah, P.B., Pundarikakshudu, K., 2006. J. AOAC Int. 89(4), 987-994.

Shah, P.M., 2002. Int. J. Antimicrob. Agents 19(2), 163-164.

Sweetman, S.C., 2002. The Complete Drug Reference, 33 ed. Pharmaceutical Press, London.

Tans, S., Verschueren, A., Dekker, C., 1998. Nature 393, 49-52.

Uzun, L., Say, R., Unal, S., Denizli, A., 2009a. J. Chromatogr. B 877(3), 181-188.

Uzun, L., Say, R., Unal, S., Denizli, A., 2009b. Biosens. Bioelectron. 24(9), 2878-2884.

Üstündağ, Z., Solak, A.O., 2009. Electrochim.Acta 54(26), 6426-6432.

Williams, J.D., Naber, K.G., Bryskier, A., Høby, N., Gould, I.M., Periti, P., Giamarellou, H., Rouveix, B., 2001. Int. J. Antimicrob. Agents 17(6), 443-450.

Yola, M.L., Atar, N., 2014. Electrochim. Acta 119, 24-31.

Yola, M.L., Eren, T., Atar, N., 2014a. Sens. Actuators B 195, 28-35.

Yola, M.L., Gupta, V.K., Eren, T., Şen, A.E., Atar, N., 2014b. Electrochim. Acta 120, 204-211.

Yola, M.L., Uzun, L., Özaltın, N., Denizli, A., 2014c. Talanta 120, 318-324.

Yu, S.S.C., Tan, E.S.Q., Jane, R.T., Downard, A.J., 2007. Langmuir 23(22), 11074-11082.

Figure Caption

Scheme 1. The procedure for fabrication of the MIP/Fe@AuNPs/2-AET-f-MWCNs/AP/GC surface

Fig. 1. (A) Modification voltammogram of 1.0 mM p-nitrophenyl diazonium tetrafluoroborate on GC electrode in 0.1 M TBATFB, at a scan rate of 100 mV s^{-1}; (B) Surface voltammogram of NP/GC electrode in 0.01 M HCl vs. Ag/AgCl/KCl_{sat}, at a scan rate of 100 mV s^{-1}; (C) Cyclic voltammograms for the electrochemical polymerization of pyrrole (80 mM) in the presence of CEF (20 mM) in phosphate buffer solution (pH 6.0) at scan rate of 100 mV s^{-1} for 9 cycles

Fig. 2. SEM images of (A) bare GC, (B) AP/GC, (C) f-MWCNs/AP/GC, (D) 2-AET-f-MWCNs/AP/GC after modification of Fe@AuNPs, (E) MIP/Fe@AuNPs/2-AET-f-MWCNs/AP/GC surfaces

Fig. 3. (A) RAIRS spectra (a) AP/GC, (b) f-MWCNs/AP/GC, (c) Fe@AuNPs/2-AET-f-MWCNs/AP/GC surfaces; (B) Cyclic voltammograms of 1.0 mM $[Fe(CN)_6]^{3-/4-}$ in 0.1 M KCl

at (a) bare GC electrode, (b) AP/GC electrode, (c) f-MWCNs/AP/GC electrode, (d) AuNPs/2-AET-f-MWCNs/AP/GC electrode, (e) Fe@AuNPs/2-AET-f-MWCNs/AP/GC electrode, (f) MIP/Fe@AuNPs/2-AET-f-MWCNs/AP/GC electrode, (g) MIP/Fe@AuNPs/2-AET-f-MWCNs/AP/GC electrode after the elution of CEF molecules, (h) MIP/Fe@AuNPs/2-AET-f-MWCNs/AP/GC electrode after the rebinding of CEF molecules; (C) Cyclic voltammograms of 1.0 mM $[Fe(CN)_6]^{3-/4-}$ in 0.1 M KCl at (a) bare GC electrode, (b) Fe@AuNPs/2-AET-f-MWCNs/AP/GC electrode, (c) NIP/Fe@AuNPs/2-AET-f-MWCNs/AP/GC electrode; (D) EIS response of 1.0 mM $[Fe(CN)_6]^{3-/4-}$ solution in 0.1 M KCl at (a) bare GC electrode, (b) MIP/Fe@AuNPs/2-AET-f-MWCNs/AP/GC electrode, (c) MIP/Fe@AuNPs/2-AET-f-MWCNs/AP/GC electrode after the elution of CEF molecules; (E) SWV curves of different electrodes after binding of 10.0 nM CEF at (a) MIP/Fe@AuNPs/2-AET-f-MWCNs/AP/GC, (b) Fe@AuNPs/2-AET-f-MWCNs/AP/GC, (c) 2-AET-f-MWCNs/AP/GC, (d) bare GC, (e) NIP/Fe@AuNPs/2-AET-f-MWCNs/AP/GC. Medium: pH 6.0 of phosphate supporting electrolyte

Fig. 4. Effect of (A) the concentration of Fe@AuNPs, (B) pH, (C) mole ratio of CEF molecule to pyrrole monomer, (D) elution time (in the presence of 10.0 nM CEF)

Fig. 5. (A) SWV curves of the imprinted electrochemical biosensor towards different CEF concentrations in pH 6.0 of phosphate supporting electrolyte; (B) The calibration curve of CEF; (C) SWV results of imprinted electrochemical biosensor towards 10.0 nM CEF, CEP, COP and COT

Highlights

- We developed molecular imprinted electrochemical biosensor for detection of cefexime
- The proposed method was validated according to the ICH guideline

- The developed electrochemical biosensor was applied to human plasma samples
- The excellent long-term stability and reproducibility of the imprinted electrodes make them attractive.
- The biosensor showed a much lower limit of detection with high selectivity.

Scheme 1

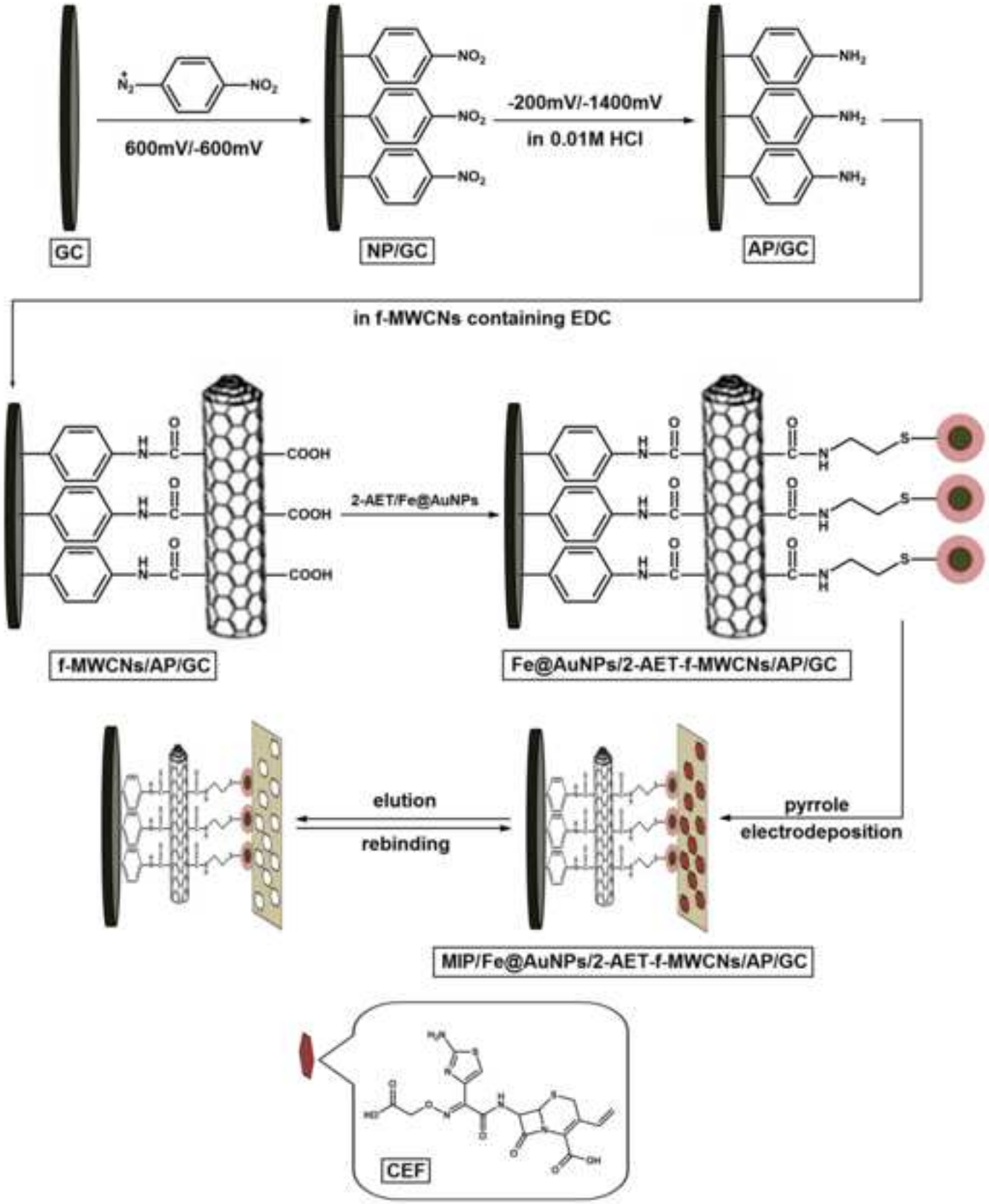

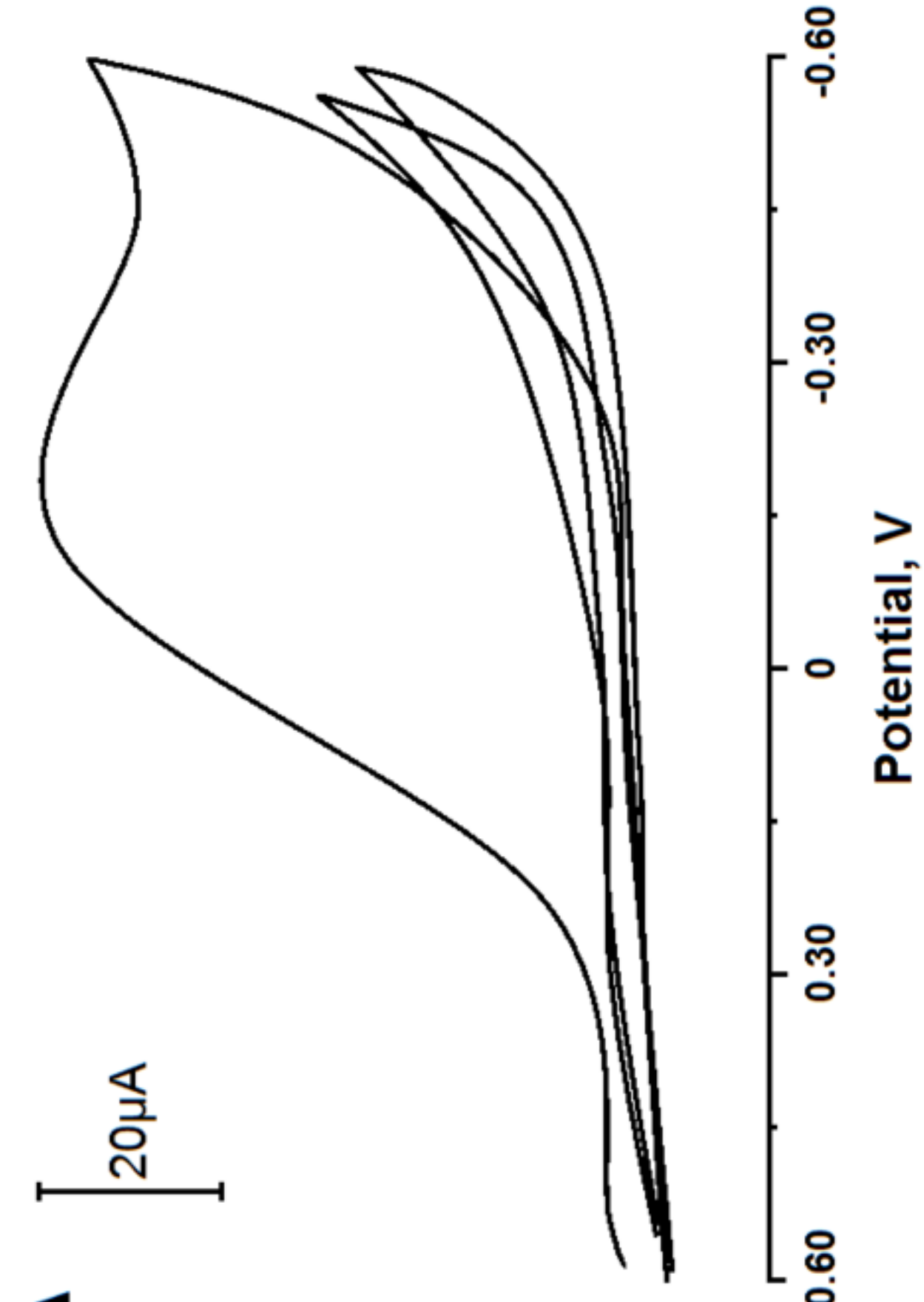

Figure 1A

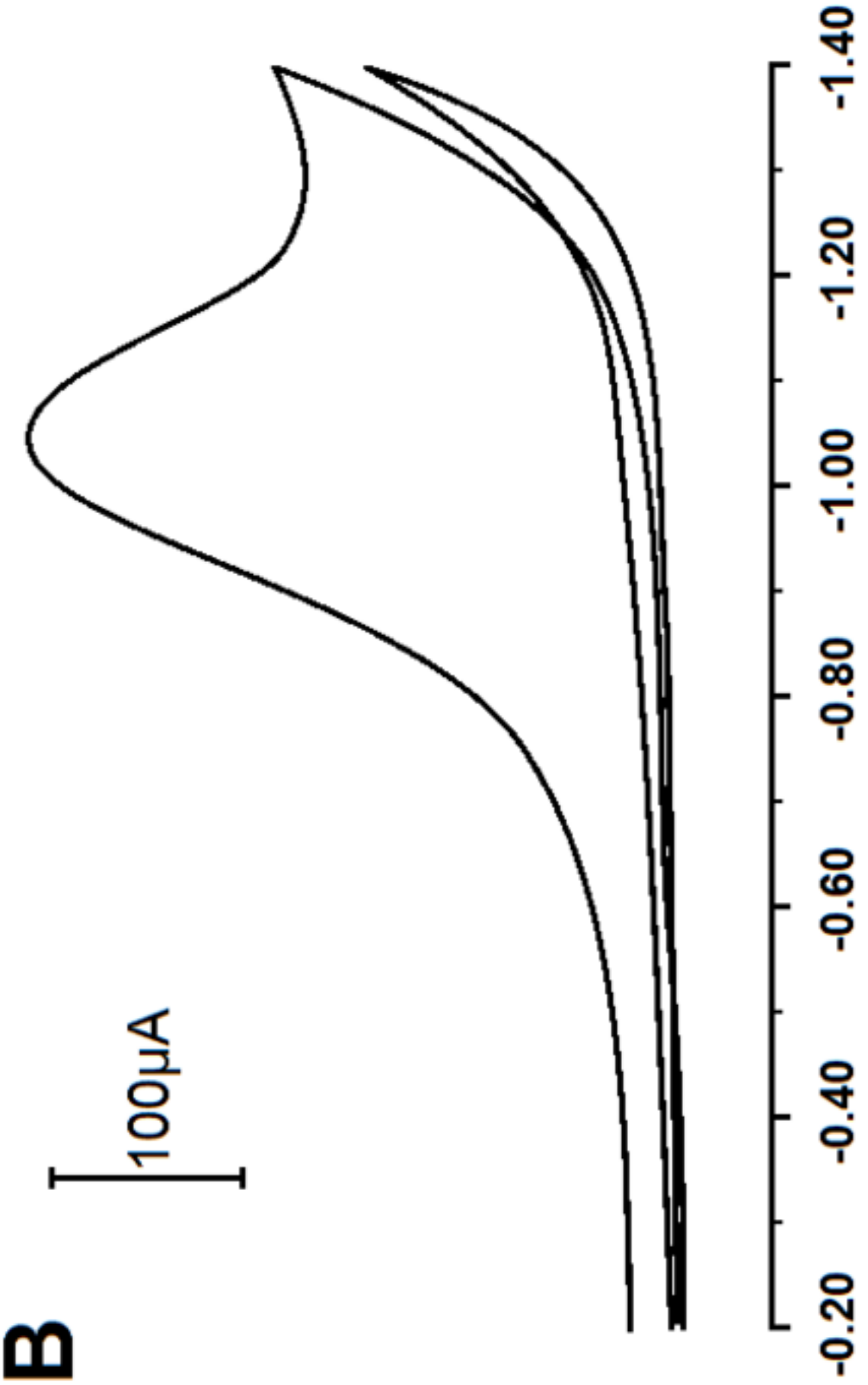

Figure 1B

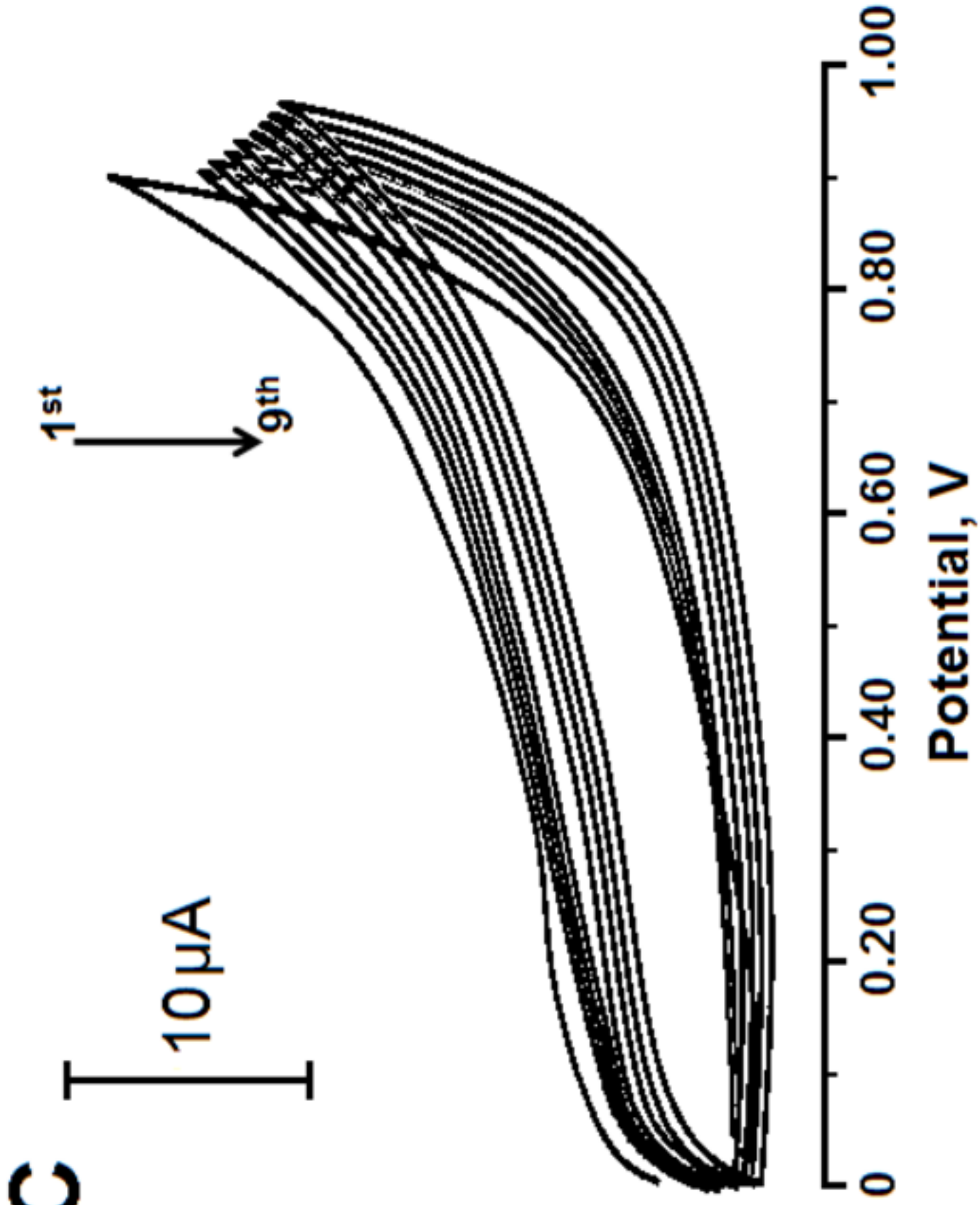

Figure 1C

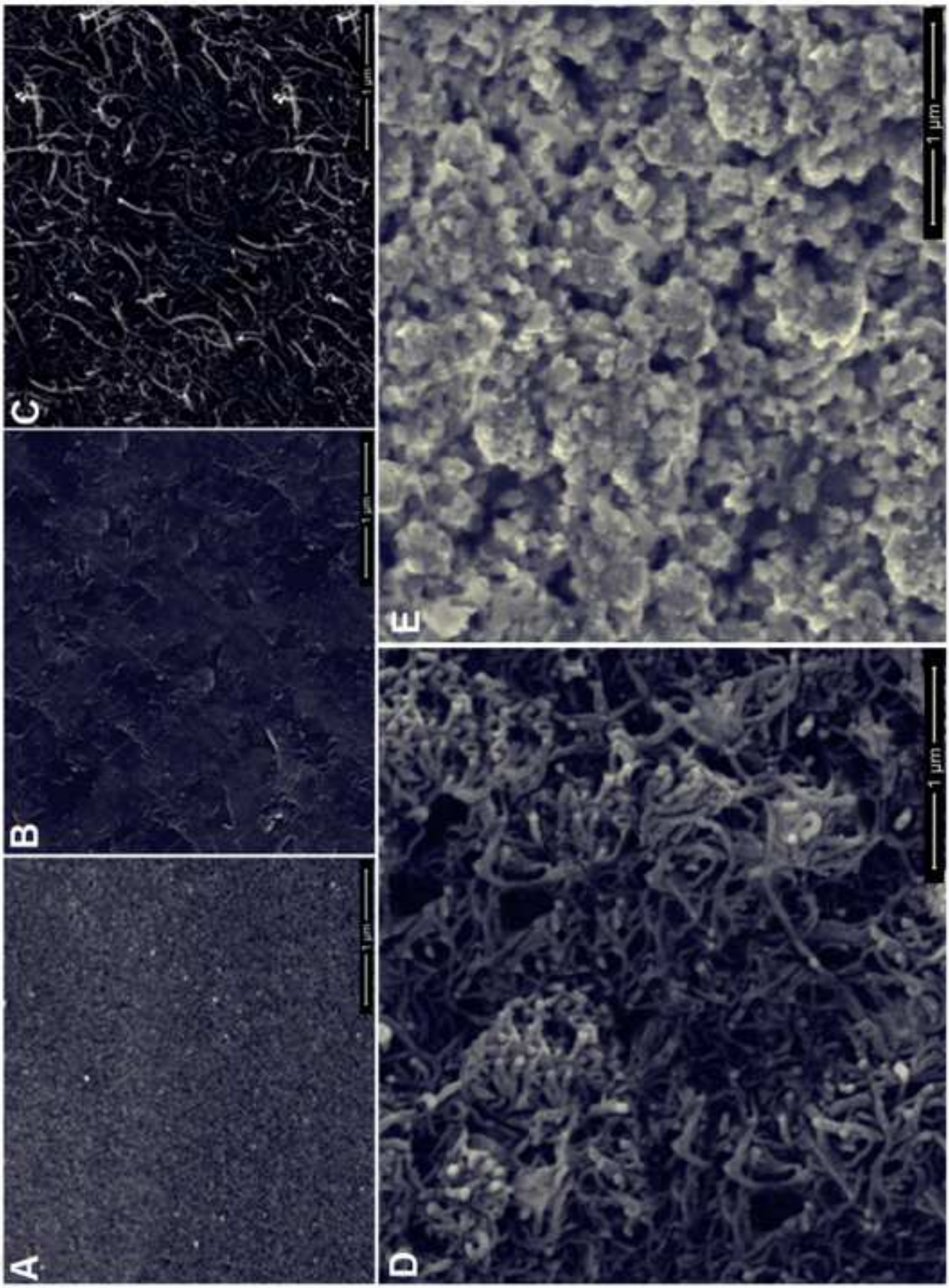

Figure 2

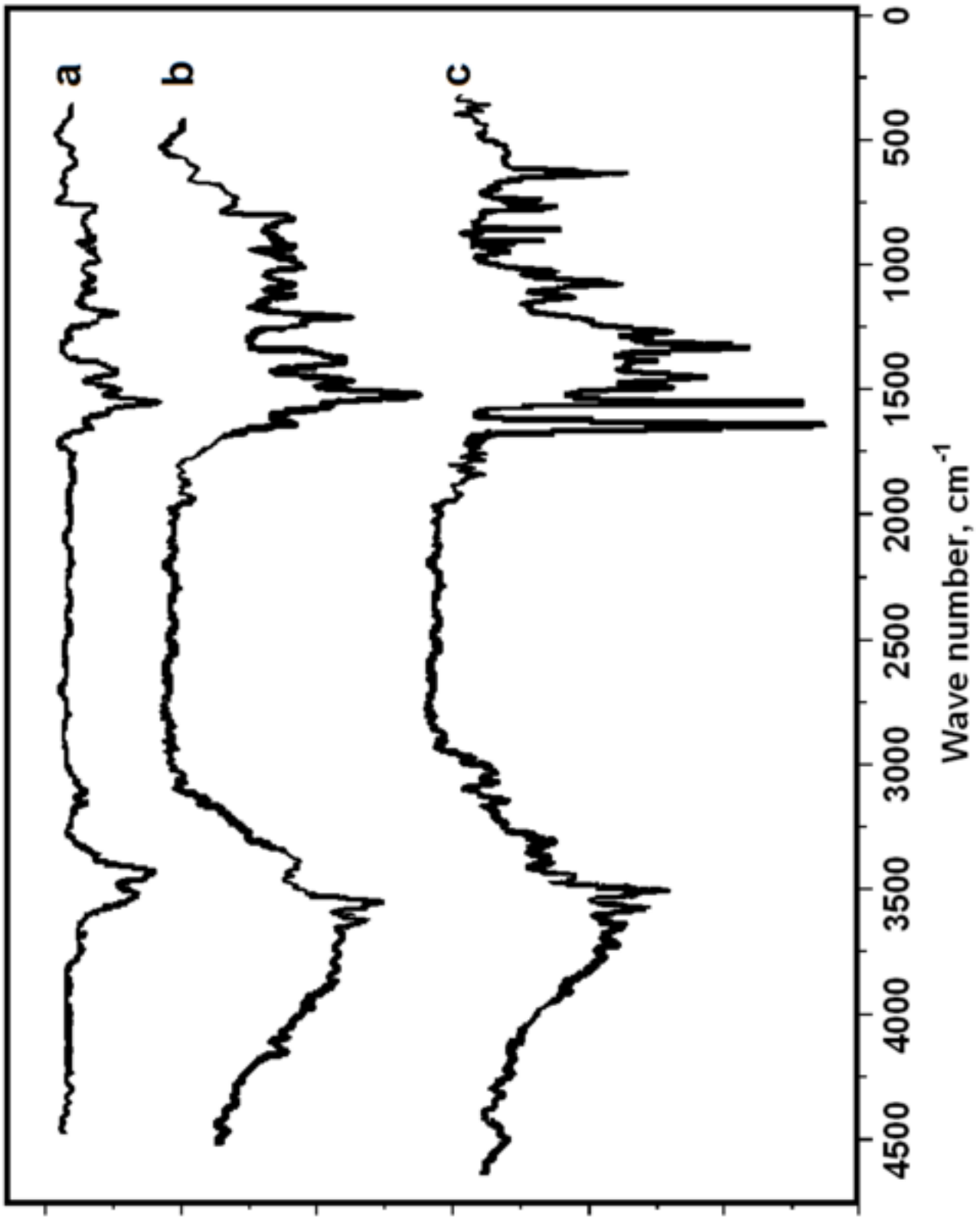

Figure 3A

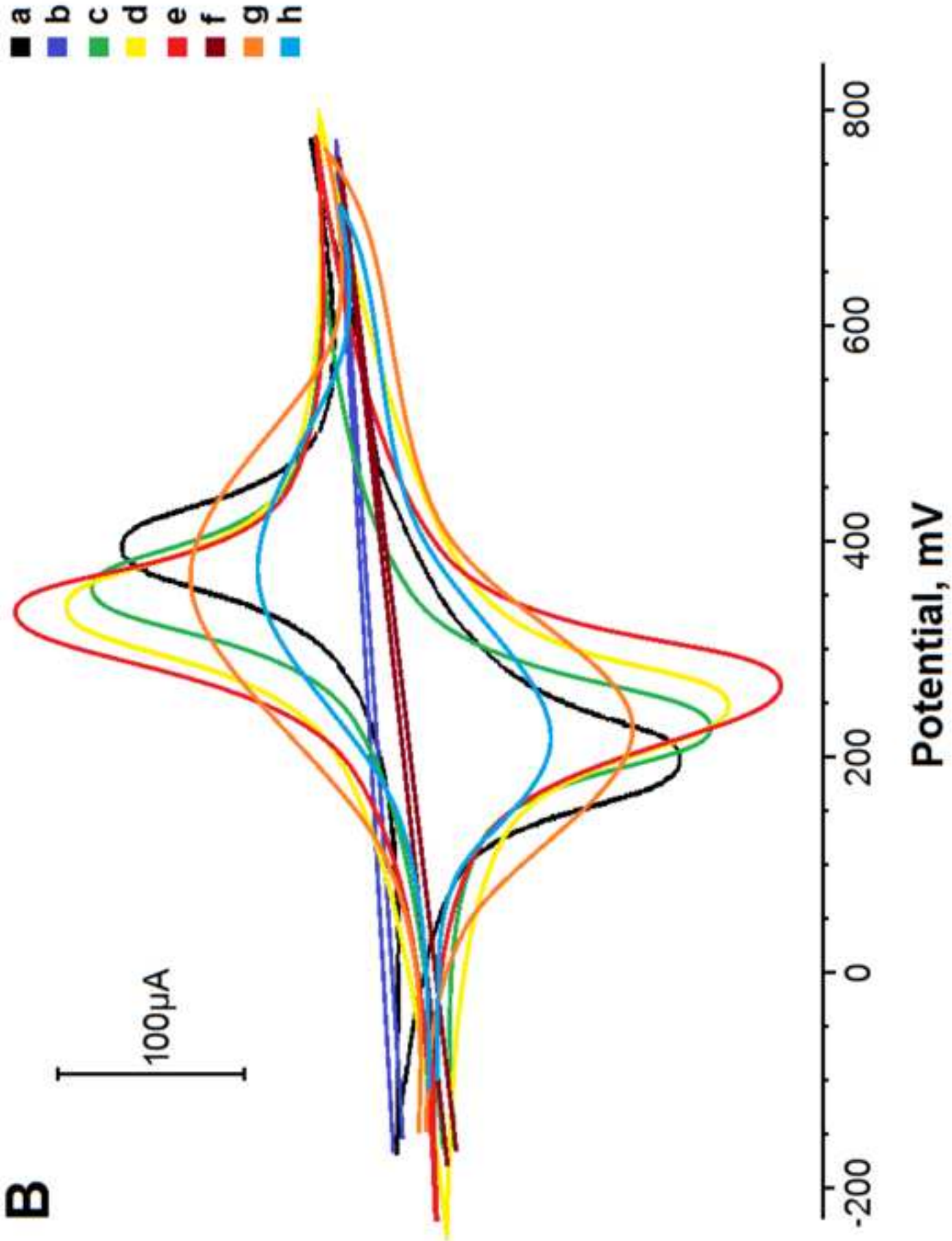

Figure 3B

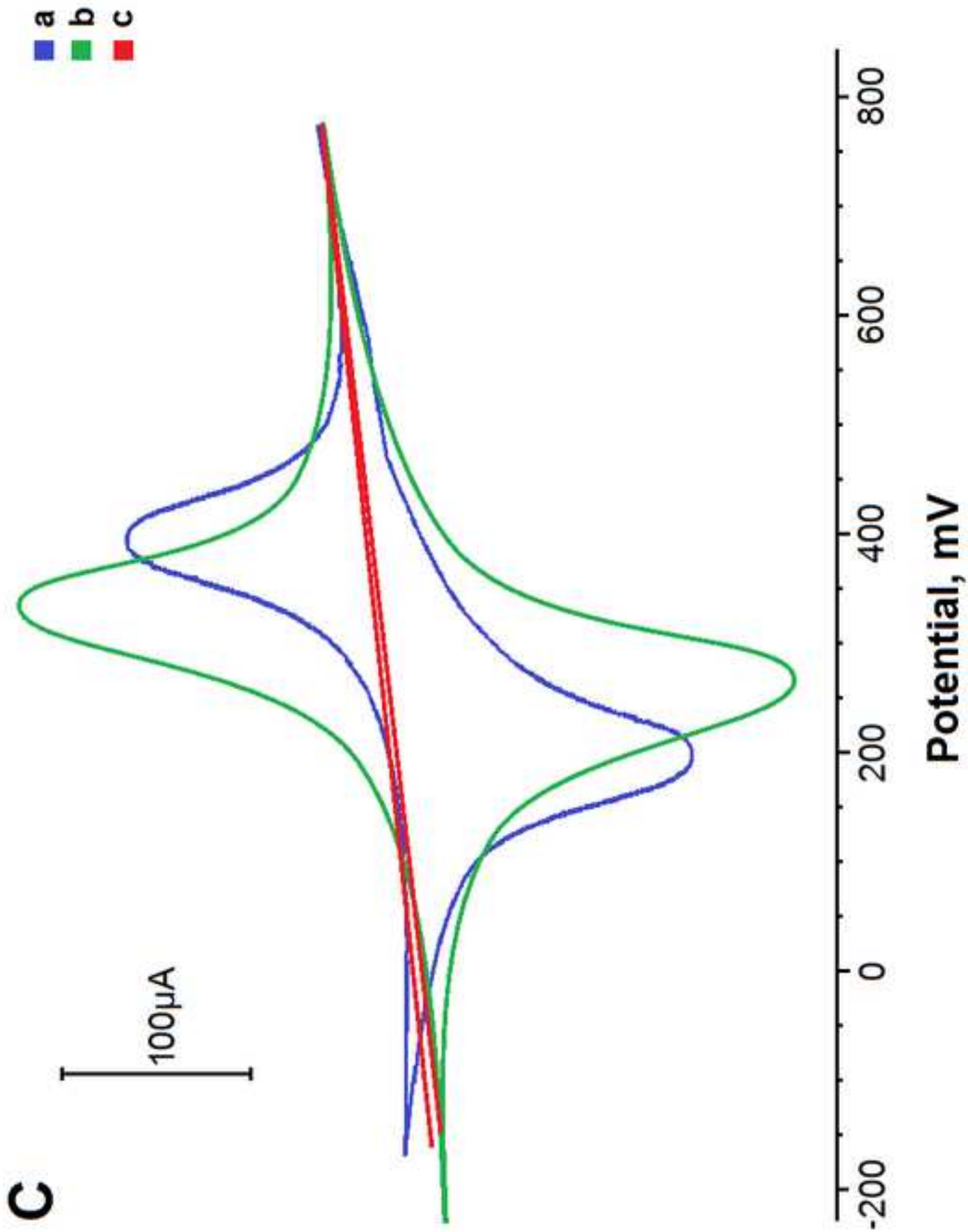

Figure 3C

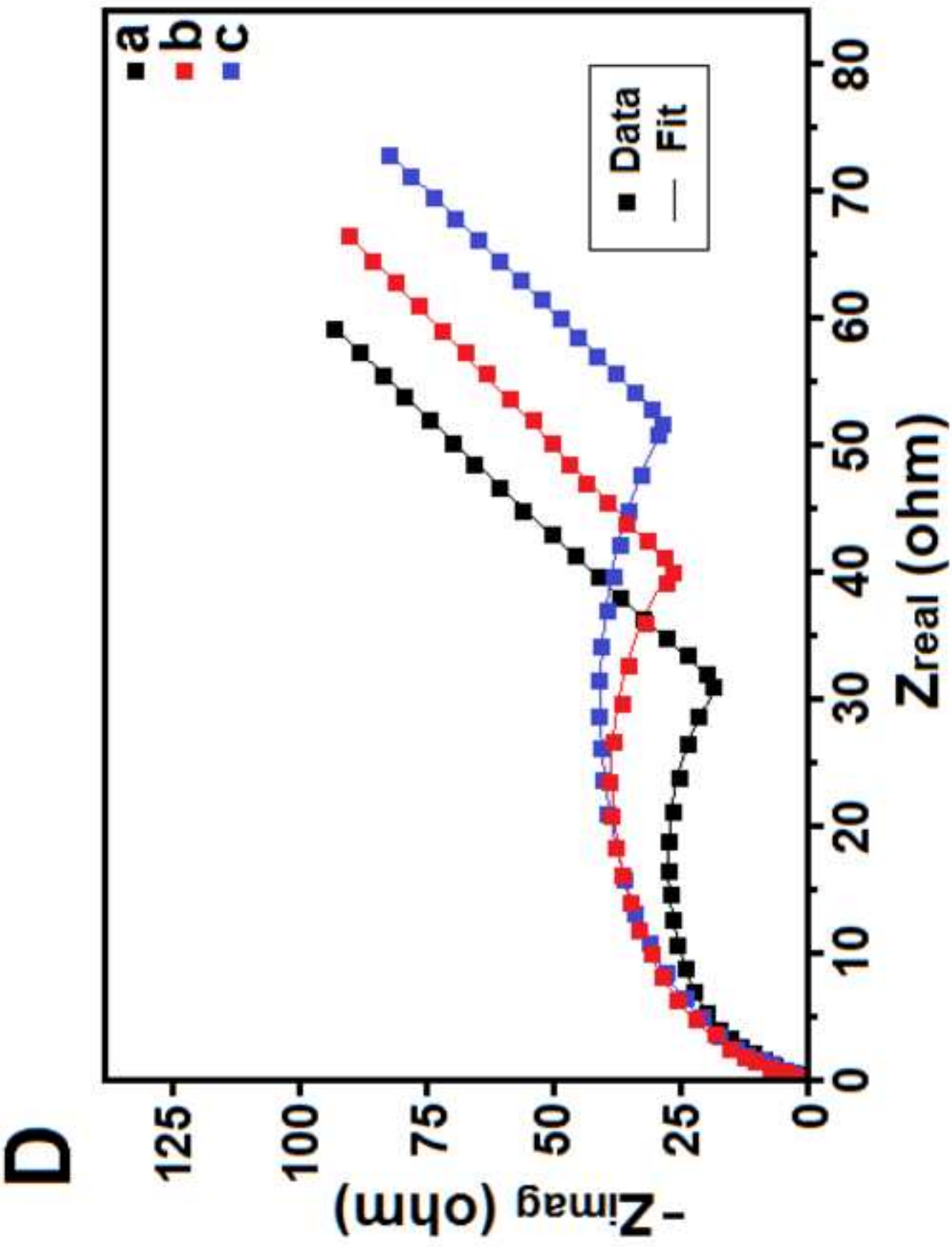
D
a
b
c
Data
Fit
-Zimag (ohm)
Zreal (ohm)
0
25
50
75
100
125
0
10
20
30
40
50
60
70
80

Figure 3D

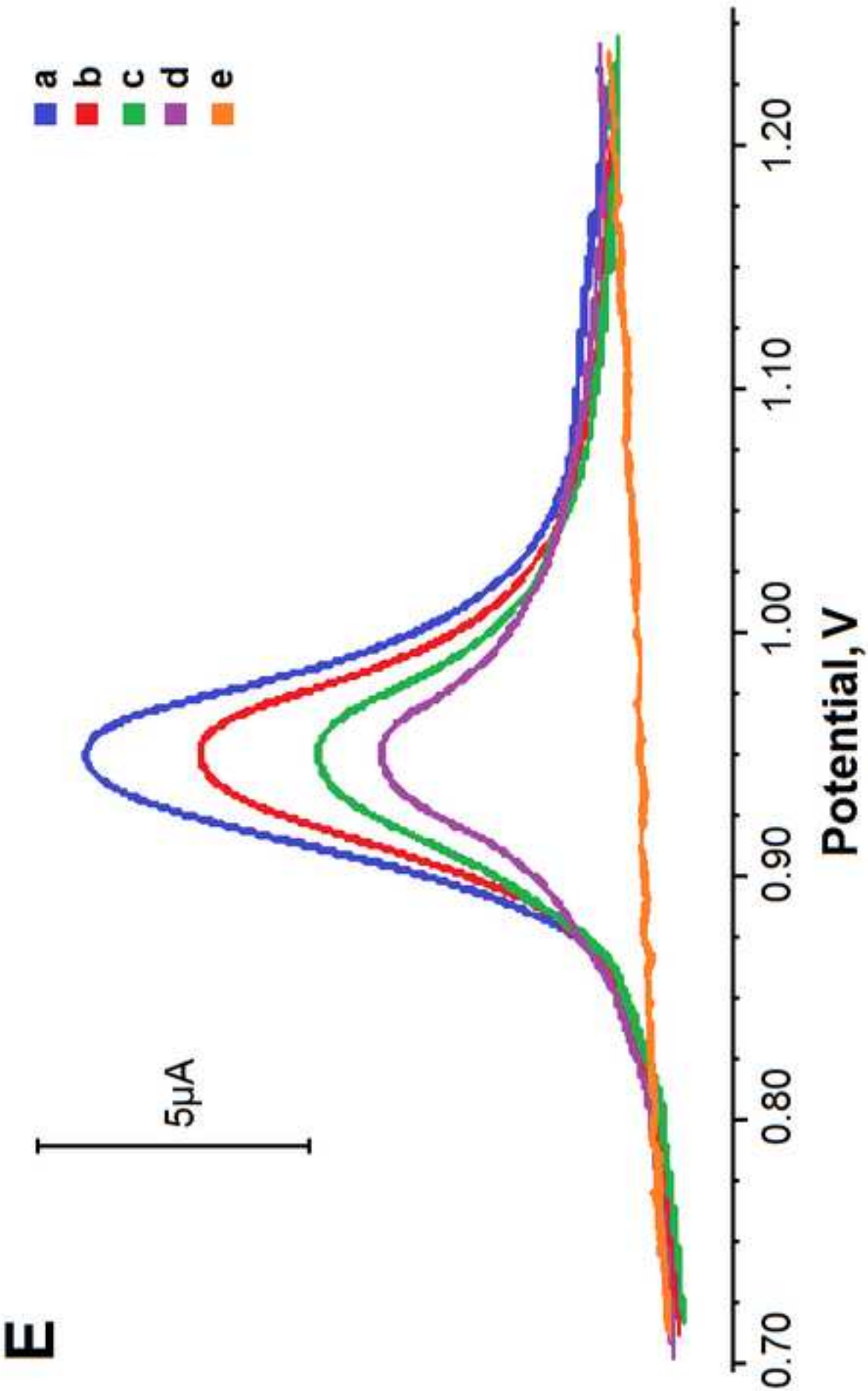

Figure 3E

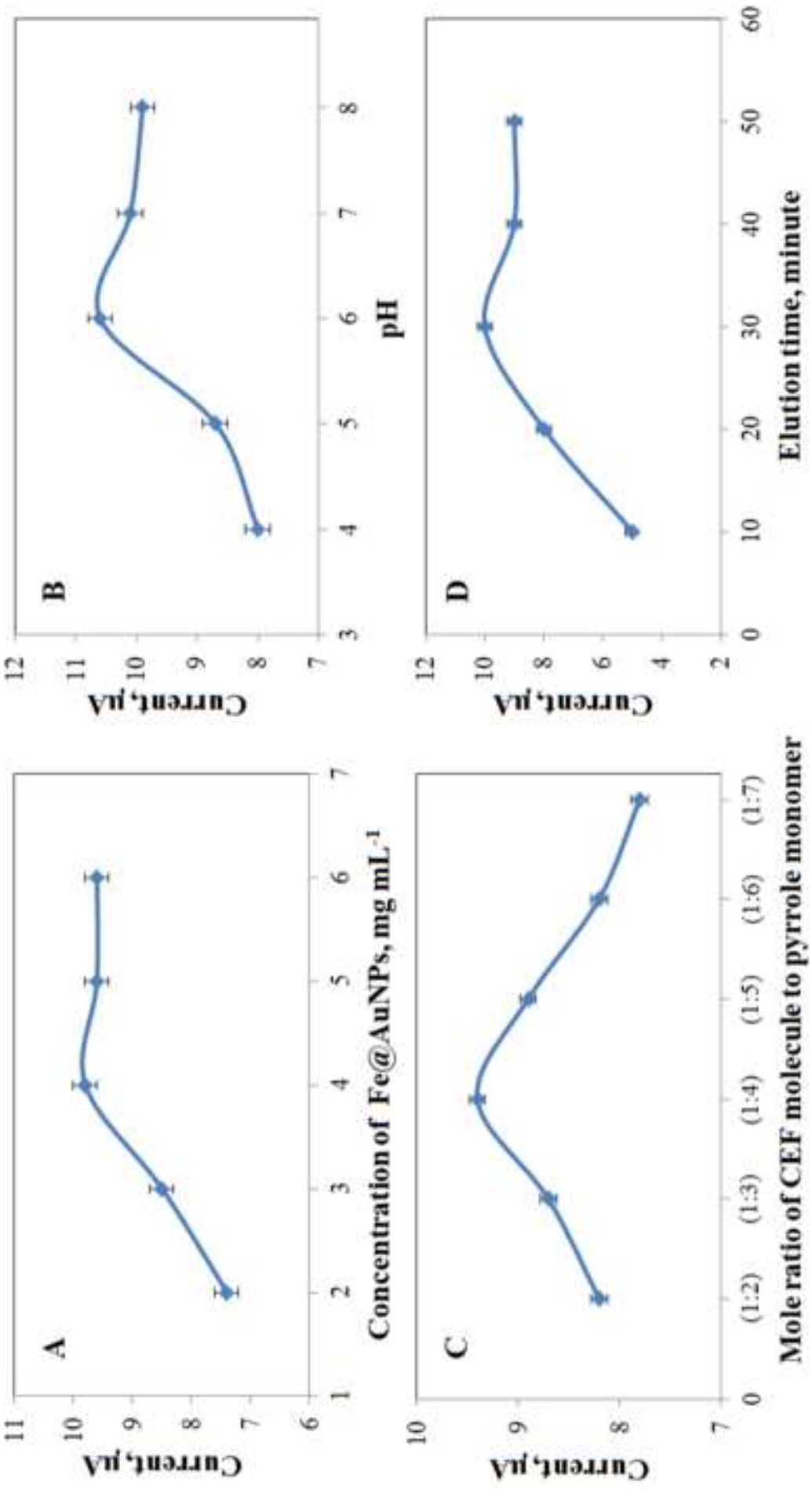
A
B
C
D
Current, µA
Concentration of Fe@AuNPs, mg mL-1
pH
Mole ratio of CEF molecule to pyrrole monomer
Elution time, minute
(1:2)
(1:3)
(1:4)
(1:5)
(1:6)
(1:7)

Figure 4

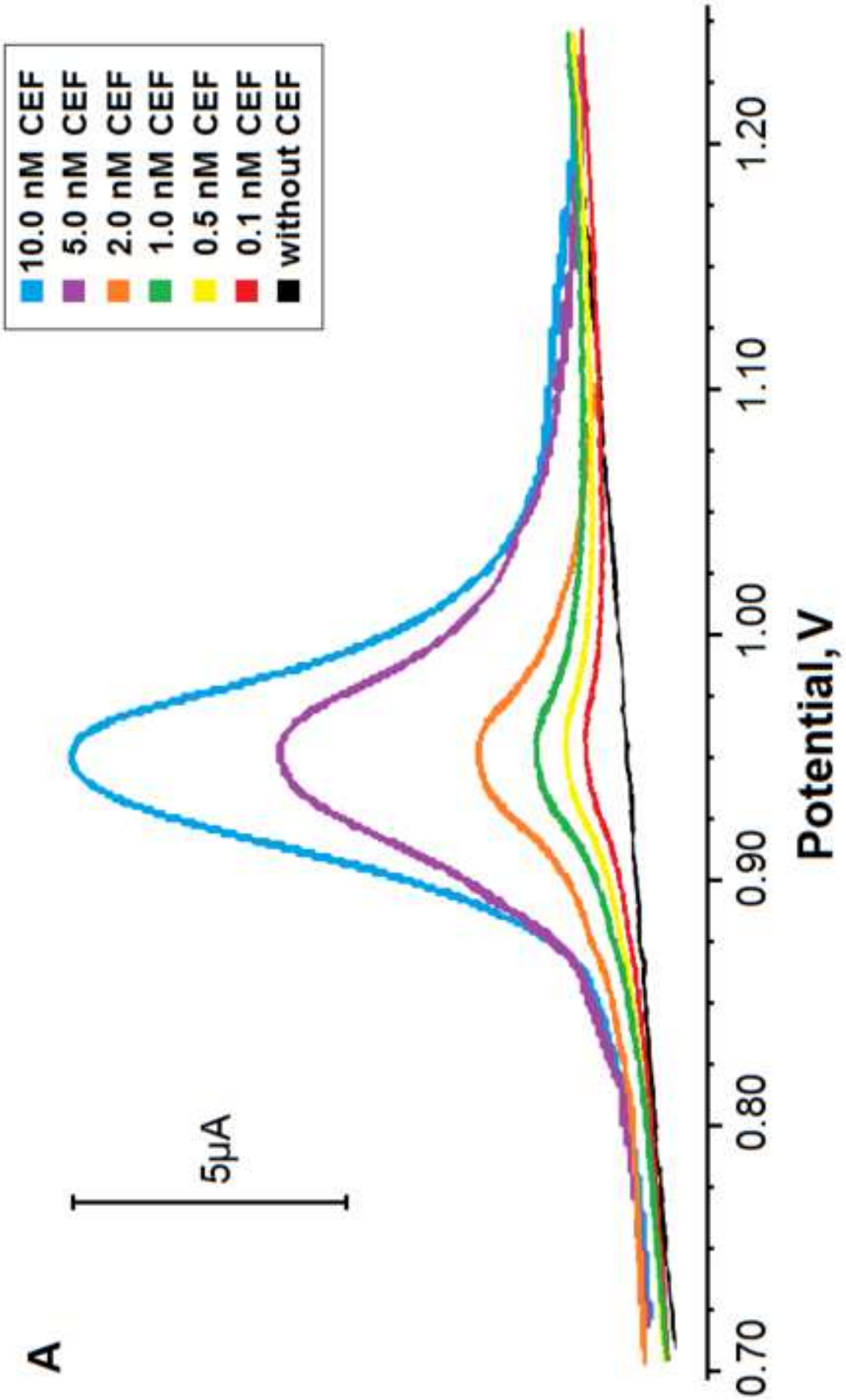

Figure 5A

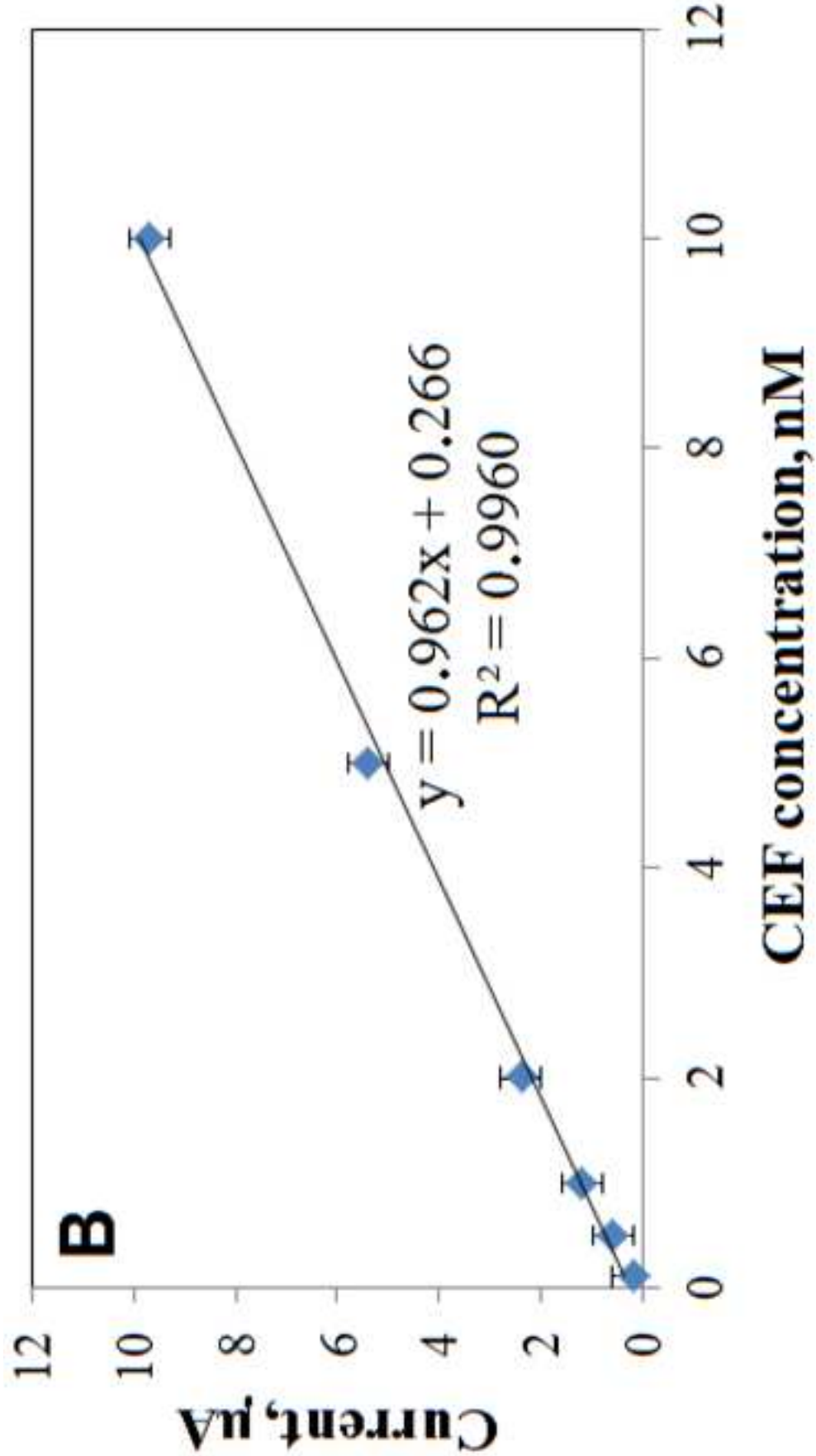
B
y = 0.962x + 0.266
R² = 0.9960
Current, μA
CEF concentration, nM
0
2
4
6
8
10
12

Figure 5B

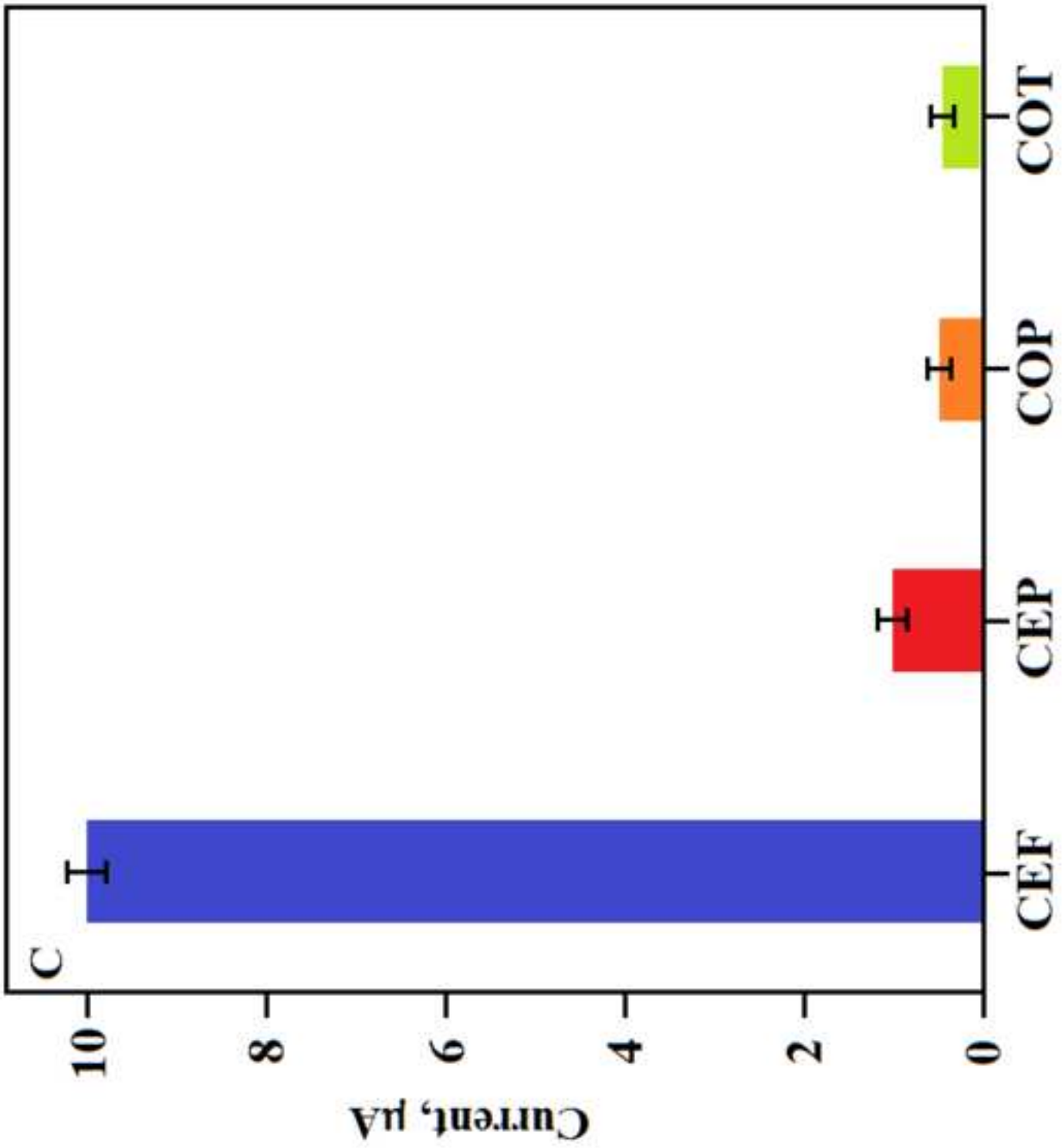

Figure 5C